Low-cost, low-profile wide-band radar cross section reduction using dual-concentric phase gradient modulated surface

Terms of use:

Publisher copyright

(Article begins on next page)

25 April 2024

Article

Low-Cost, Low-Profile Wide-Band Radar Cross Section Reduction Using Dual-Concentric Phase Gradient Modulated Surface

Yousef Azizi [1,2], **Mohammad Soleimani** [1], **Seyed Hasan Sedighy** [3] **and Ladislau Matekovits** [2,4,5,*]

1   Department of Electrical Engineering, Iran University of Science and Technology, Tehran 1684613114, Iran; yousefazizi@elec.iust.ac.ir (Y.A.); soleimani@iust.ac.ir (M.S.)
2   Department of Electronics and Telecommunications, Politecnico di Torino, Corso Duca degli Abruzzi 24, 10129 Turin, Italy
3   School of New Technologies, Iran University of Science and Technology, Tehran 1684613114, Iran; sedighy@iust.ac.ir
4   Istituto di Elettronica e di Ingegneria dell'Informazione e delle Telecomunicazioni, National Research Council of Italy, 10129 Turin, Italy
5   Department of Measurements and Optical Electronics, University Politehnica Timisoara, 300006 Timisoara, Romania
*   Correspondence: ladislau.matekovits@polito.it; Tel.: +39-011-090-4119

Abstract: Design criteria of low-cost, dual-concentric metasurface possessing wideband phase gradient (PG) are introduced. The radar cross-section reduction (RCSR) is explained by anomalous reflection that characterizes the superficial planar. The geometry consists of two single band RCSR modulated surfaces (MSs) that are triggered in each other. Each MS is built-up of square patch (SP) unit cells configured as a modulation structure to realize PG that causes anomalous reflection and monostatic RCSR behavior. Applying sinusoidal modulation to the sequence of the SP unit cells leads to the formation of PG along the surface and hence the intensity of the reflected wave is reduced for the broadside direction ($\theta_r = 0°$). The proposed structure fabricated on a 0.8 mm thin FR-4 substrate extends over 249×249 mm^2. It achieves a wide RCSR bandwidth from 20.9 GHz to 45.7 GHz (i.e., relative bandwidth of 75%) as designed in Dassault Systèmes (CST) Microwave Studio as a full-wave simulator and confirmed by the measurement results.

Keywords: phase gradient; radar cross section reduction; square patch unit cell; modulated surface

1. Introduction

RCSR by phase gradient metasurface (PGM) has attracted considerable attention in recent years. Unlike the phase cancellation method that uses two unit cells with phase variation of $\pm 37°$ around $180°$ [1–3], in the PGM design several unit cells with phase difference less than $|180° \pm 37°|$ between them are considered. The operational principal of PGM is based on two different phenomena: (i) anomalous reflection and (ii) surface wave conversion, achieving the ability to reduce the reflected power [4]. By using large number of unit cells in the metasurface structure, phase differences between adjacent unit cells were decreased and 74% RCSR bandwidth has been achieved by thick (2.5 mm) substrate [5]. By controlling the anomalous and diffuse reflection parameters in modified unit cells, the PGM metasurface can also be designed as an antenna superstrate [6]. Although the RCSR bandwidth increased up to 82.4% without degradation of the antenna performance, the high thickness substrate (3 mm) limits its practical applications. By using hybrid resonant structure, a dual band PGM with anomalous reflection mechanism presented both theoretically and experimentally (with substrate thickness of 0.5 mm) is able to reduce the backscattering RCS of the surface for two frequencies, namely for 8.9 and 11.4 GHz [7]. Narrow bandwidth performance, i.e., lower than 2% at each band is considered as a

limitation on practical applications. In [8], the chessboard structure with 77% RCSR bandwidth using holographic surface (HS) and MS redirector is introduced such that each of the MS and HS reduce the RCS in a single band; by placing them in a chessboard configuration, wideband RCSR is achieved. Although the structure is simple and low-cost, its substrate thickness is still relatively high (1.6 mm). It is also possible to create a PGM with coded PGM (CPGM). Using holographic surfaces to convert the impinging wave into surface one, as well as anomalous or diffuse reflection of the incidence, RCSR can be achieved as introduced, for example [9], that suffer from low bandwidth. In 2017 Zheng et al. introduced a concept of CPGM that it is more flexible to manipulate the reflected wave by changes of the coded configuration [10]. Although wide angle RCSR performance highlighted the use of this CPGM structure, RCSR bandwidth (lower than 64%) and 3 mm substrate thickness are their issues. In another effort by applying the modulation to the coding element and coding sequence simultaneously, two dimensional CPGM has been developed that presents a more flexible pattern manipulation [11]. However, the low bandwidth (46%) is a disadvantage of this structure. By using 4 bit optimized coded metasurface, RCSR bandwidth improved up to 91% [12]. Even though the RCSR bandwidth is enough for practical application, it uses a high cost substrate (F4B). In [13] by using amplitude and phase gradient modulated surface (APGM), RCSR improvement was achieved with 128% bandwidth. Using amplitude gradient as an auxiliary variable caused the RCSR bandwidth improvement simultaneously with improvement of RCS depth. Even though the structure has an ultra-wideband RCSR performance, their dual layer thick substrate (3.2 mm) is considered as a disadvantage.

In this letter, a new dual concentric phase gradient modulated surface (PGMS) is introduced for RCS reduction at wideband frequency range, 20.9–45.7 GHz (75%). In this concentric surface, the anomalous reflection is employed as the main RCS reduction mechanism. The introduced structure consists of two single band concentric modulated surfaces, MS1 and MS2, which reduce RCS from 20.5–32 GHz (45%) for MS1 and 31.8–46.5 GHz (40%) for MS2, consequently. In both MS1 and MS2, RCSR formation is based on gradual phase difference between adjacent unit cells. The square patches (SPs) unit cell is used with sinusoidal pattern for both MS1 and MS2 by changing cell gap size (contrarily to the usual change in the patch size). By placing MS2 in the central part of MS1, a concentric configuration is obtained that exhibits wideband 75% (20.9–45.7 GHz) RCSR performance. The proposed surface has significant advantages with respect to the state of the art references such as low-cost, very low profile (0.8 mm thin), simple manufacturing process (by standard microstrip technology) and wideband monostatic RCSR performance.

2. PGM Design

Based on the generalized Snell's law, the existence of PG along the *x* and/or *y* directions in a given coordinate system (see Figure 1) leads to the reflection of an incident wave with incidence angle θ_i (with respect to the normal $\hat{z}$) in the direction θ_r (reflection angle of the scattered wave), where the two angles are related by Equation (1) [14]:

$$\sin(\theta_r) - \sin(\theta_i) = \frac{1}{k_0}\frac{d\Psi_{x,y}}{d_{x,y}} \tag{1}$$

where k_0 is the free space wave number and $\frac{d\Psi_{x,y}}{d_{x,y}}$ defines the PG along the *x,y* coordinate.
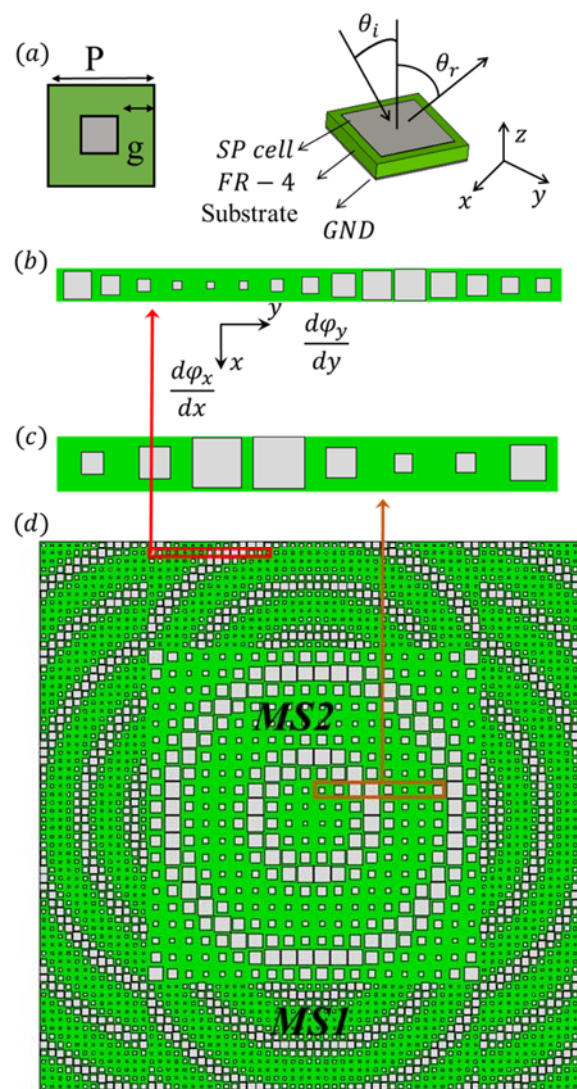
Figure 1. (**a**) SP unit cell, (**b**) PG formation by sinusoidal modulation applied to the MS1 and (**c**) MS2, (**d**) CAD model of the dual-concentric configuration.

According to Equation (1), considering a normally incident plane wave ($\theta_i = 0$) that illuminates the MS with PG characterized by a sinusoidal modulation leads to $\theta_r > 0°$. In the case of constant PG value, constant reflection phase ($\theta_r =$ const.) occurs which can be useful in some practical applications. However, in the case of monostatic RCSR, not only constant PG but variable PG along the *x,y* directions could make arbitrary reflections that decrease the backscattering of the incident waves. In fact, by assuming $\theta_i = 0$ and $\frac{d\Psi_{x,y}}{d_{x,y}} \neq 0$ according to Equation (1) the reflection angle can be expressed as:

$$\theta_r = \arcsin\left(\frac{1}{k_0}\frac{d\Psi_{x,y}}{d_{x,y}}\right) > 0 \tag{2}$$

Based on Relation 2, the design of the metasurface with wideband non-zero PG causes the reflected signal being in opposite direction with the incident one and this is enough for monostatic RCSR achievement. Therefore, sinusoidal modulation is applied into SP unit cell to form a PG and reflection on arbitrary direction, consequently as depicted in Figure 1. The introduced PGM consists of dual concentric MSs (MS1 and MS2) which is plotted in Figure 1d. For the arrangement of the final structure (Figure 1d), Matlab and Dassault Systèmes (CST) Microwave studio was used. By linking Microwave Studio with Matlab the dual concentrate structure was built in the simulation environment and analyzed in

full-wave structure that was discussed in [8–13]. Resizing the SP gaps in Figure 1 is based on the formation of the appropriate PG and redirecting the input wave. In fact, the tradeoff between maximum RCSR bandwidth, wave redirection and structure dimensions is done by an optimization process. In each MSs, the sinusoidal modulation is applied to the SP unit cell to reduce the RCS in a certain bandwidth, indicated by Δf_1 and Δf_2, respectively. SP unit cells are placed on the grounded FR-4 substrate with $\varepsilon_r = 4.4$, $\tan \delta = 0.025$ and of 0.8 mm thickness. Due to the reduced thickness of the supporting dielectric and presence of the ground plane, the unit cell reflects the total incident power. Therefore, the reflection phase can be considered as the main degree of freedom in the unit cell design that gradually changes with the gap size between patches. As depicted in Figure 1a, the following relation $g = (P - d)/2$ between cell parameters is considered, where d and g correspond to the length of the patch and gap size, respectively. The period (P) of the unit cells in MS1, MS2 is 3.5 mm and 7.1 mm, respectively. Two MS1 and MS2 dimensions were extracted by full-wave (CST Microwave Studio) simulations that lead to the gradual phase difference between SP unit cells. Because of the SP symmetry with respect to x, y, and using sinusoidal modulation, MS1 and MS2 PG values are the same. Reflection phase of the MS1 and MS2 are plotted in Figure 2, with the gaps size of 0.2, 0.5, 0.9, 1.4, 1.6 mm and 0.4, 0.8, 1.4, 2, 2.5 mm, respectively. It is observed that MS1 (solid lines) in the 20–33 GHz band has a non-constant PG versus radial distance which can be helpful for monostatic RCSR. In a similar manner, MS2 (dashed lines) exhibits similar behavior in 33–45 GHz band. Based on Equation (2), in case of non-constant PG ($\frac{d\Psi_{x,y}}{d_{x,y}} \neq 0/const.$) along the x,y direction it is expected that the reflected wave can be redirected in different directions with respect to the incident one. While constant PG leads redirecting of the reflected wave into a specific direction, the non-constant PG cause the redirection of the incidence wave in all directions and of effective monostatic RCSR, consequently.
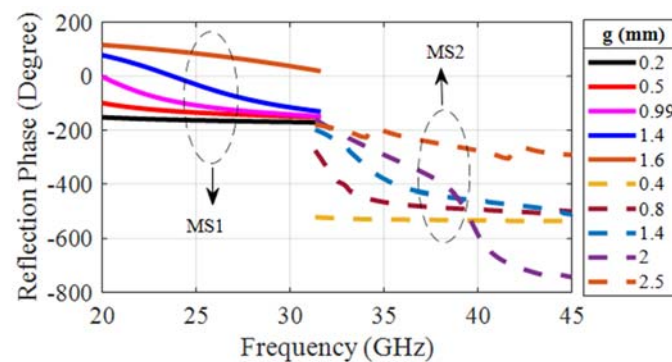

Figure 2. Reflection phase of MS1 (Solid Lines) and MS2 (dashed lines) versus gap variation of the cells.

To prove the idea, two MS1 and MS2 RCS simulation results are plotted in Figure 3a versus frequency: both MS1 and MS2 exhibit the expected behavior for PG with the variation of unit cell gap size in the $\Delta f_1 = 31.8 - 46.5$ GHz (40%) and $\Delta f_2 = 20.5 - 32$ GHz (45%) frequency bands, respectively. In both MS1 and MS2, there are certain numbers of unit cells with constant gap size and reflection phase at each constant radius (with respect to the center of the surface). By gradual change along the radius, the gap size of the cells changes in a sinusoidal fashion which leads to the PG formation that increases the monostatic RCSR by benefiting of an anomalous reflection mechanism that in turn leads to wideband monostatic RCSR. The RCS patterns of MS1 and MS2 at 28 GHz and 35 GHz for a normally incident plane wave are shown in Figure 3b,c, respectively. Based on Figure 3b,c it is observed that the maximum reflections happen in the $\varphi = 45°$ plane for both MS1 and MS2. It can be seen that both MS1 and MS2 redirect the incident plane wave to the angle of $30°$ and $16°$ (which was extracted from two-dimensional RCS simulation results of MS1 and MS2 in $\varphi = 45°$ plane), which proves the formation of anomalous reflection.
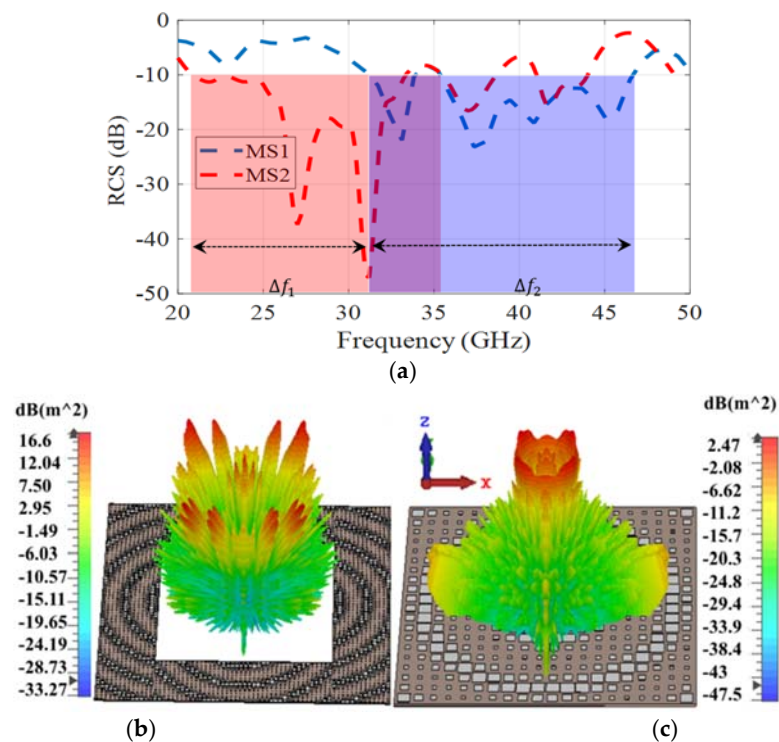
Figure 3. RCS of MS1 and MS2: (**a**) Monostatic RCS of MS1 and MS2; (**b**) RCS pattern of MS1 at 28 GHz; (**c**) RCS pattern of MS2 at 35 GHz.

3. Measurement and Results

The final dimensions of MS1 and MS2 require some optimization due to their location in the concentric composition and the total size of the structure (249×249 mm^2). As a result of the optimization aiming to obtain a better RCS bandwidth, the final MS1 and MS2 unit cells periods are changed to 3.8 and 7.5 mm, respectively. Additionally, the gap sizes of the MS1 and MS2 are 0.2, 0.6, 1, 1.3, 1.6 and 0.4, 0.9, 1.5, 2.1, 2.6 mm, respectively. It is noteworthy that the external dimension of MS1 and MS2 has been selected by a tradeoff between their surface area and wideband RCSR performance to obtain the maximum RCSR bandwidth. In Figure 4a–c the fabricated prototypes of MS1/MS2 and Tx/Rx antenna for monostatic RCS measurements are shown, respectively. In fact, MS1 and MS2 were fabricated together, and separated in a second moment by cutting the general structure, and the monostatic RCSR of each metasurface has been measured separately. The measured result in Figure 4d depicts good agreement with the simulation one. RCS measurements have been carried out using N5227A PNA network analyzer as a transmitter and receiver that cover frequency range of 10 MHz-67 GHz. The test frequency range is from 22 GHz to 42 GHz (20 GHz band). The limitation of the frequency range is due to the limitation of instruments such as waveguide feeder, horn antenna and LNA. The 20 GHz test bandwidth is divided into 1601 frequency points and the resolution bandwidth of the PNA chosen as 100 Hz to obtain the proper results in a time gating process extraction. The anechoic chamber supported the RCS measurement based on IEEE standard 1502TM and was suitable for high frequency RCSR measurement [15]. Tx/Rx antenna and dual concentrate MS have a 1.5 m height and the distance between them is about 2.5 m.
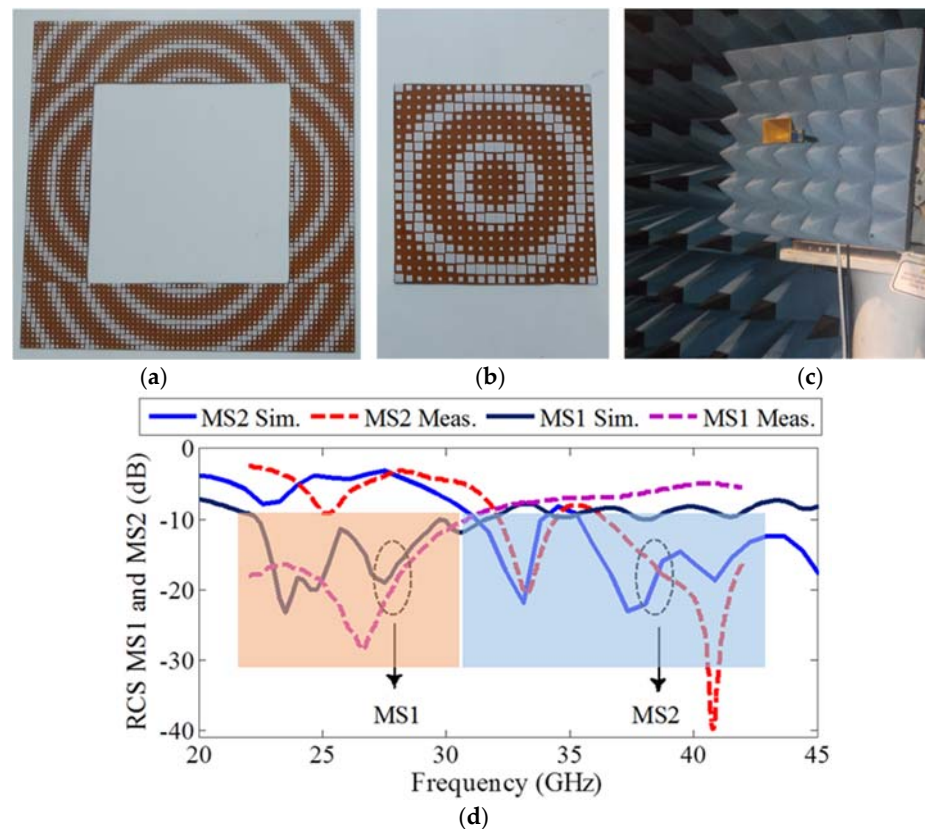
Figure 4. MS1, MS2 and their monostatic performance (**a**), (**b**) Prototype of MS1 and MS2; (**c**) wideband horn antenna as a Tx/Rx antenna; (**d**) RCS Simulation and measurement results of the MS1 and MS2.

The RCS test method based on time gating has consisted of two steps: (i) measurement of monostatic RCS of the MS1, MS2 and the dual-concentric MS structure, which is done by using a Tx/Rx antenna simultaneously and using a directional coupler to separate the forward/backward waves, and (ii) RCS pattern of the dual concentric MS is performed at 30 GHz by using Marconi set up (Figure 5a). In the Marconi test set-up, two antennas are used: the Tx antenna is placed in front of the introduced MS and the Rx antenna, which is located on the rotating and calibrated arm, and is moved manually to measure the RCS at different angles. Figure 4b shows the simulation and measurement monostatic RCSR results of MS1 and MS2.

It is noteworthy that there is some difference in the measurement results with respect to the simulated one, especially at Δf_1 frequency band, due to the existence of fabrication and measurement errors, as well as extracting the results from the time gating method and applying time filters is acceptable. Figure 5a depicts the photograph of the realized prototype that is mounted in anechoic chamber for monostatic RCS measurement. Combining the two single-band RCSR surface (MS1 and MS2) in the form of a concentric MS effectively increases the 10 dB RCS bandwidths to 20.9–45.7 GHz (75% fractional bandwidth) verified by measurement as depicted in Figure 5b. The RCS measurement (bi-static at 30 GHz) and simulation results of dual concentric MS sample shown in Figure 5c, which indicates the good agreement between simulation and measurement results. The anomalous reflection resulting from PG or gradual phase difference between the adjacent unit cells present in the MS1 and MS2 reduces the RCS of the introduced dual concentrated MS. The bi-static RCS results in the introduced structure and PEC with equal size with 1° angular step was performed at 30 GHz and plotted in Figure 5c. It can be seen that at 30 GHz the introduced dual-concentric MS achieves 23 dB RCSR compared with the PEC surface with same dimensions. For a better presentation of the results allowing an easier comparison,

the measurement and simulation results of Figure 5c are normalized with respect to 0 dB. According to the results of Figure 5c, there is good agreement between measurement and simulation for angles of 0°–15°. The measurement and simulation results have some differences of few dB between the angles of 60°–90°; however, these results are acceptable due to the low amplitude of the reflection signal at these angles relative to the main lobe.
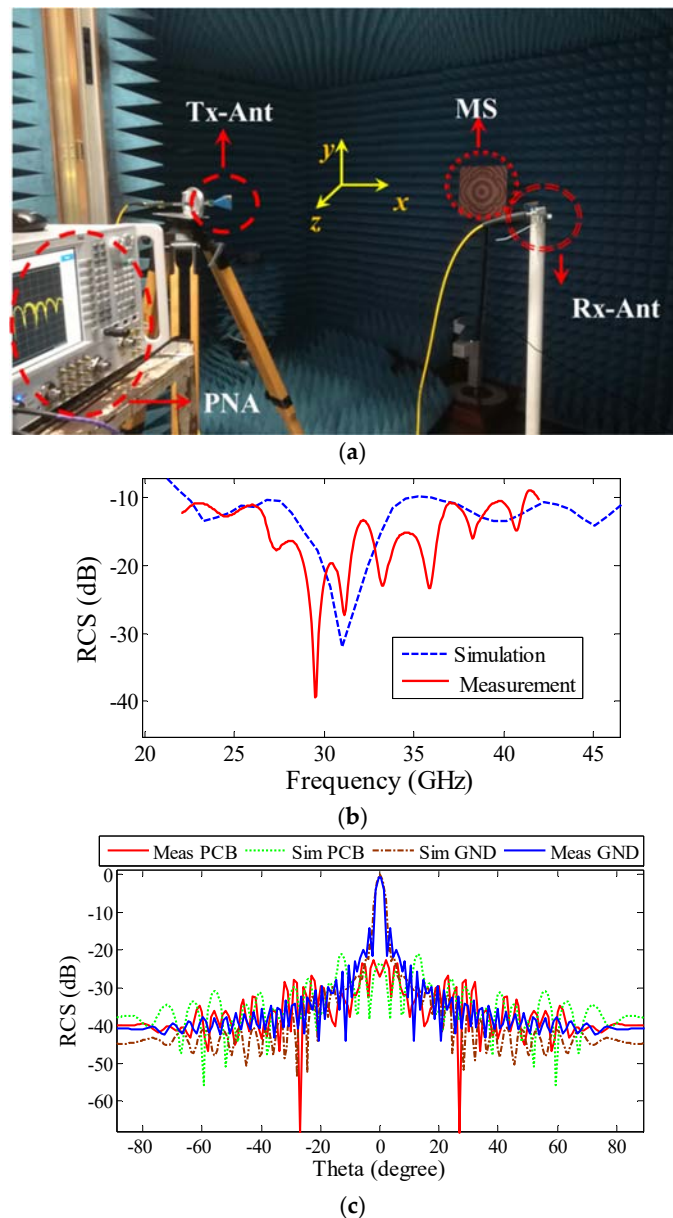

(a)

(b)

(c)

Figure 5. RCS results and test set-up: (**a**) fabricated dual concentric MS in anechoic chamber; (**b**) measurement and simulation results of monostatic RCS; (**c**) RCS of the structure vs. similar PEC surface that measured by Marconi set-up.

In order to express the features of the introduced structure, a comparison with available data from the literature is given in Table 1. Low-cost, ease of construction (thin single-layer structure with 0.8 mm thickness and no need for lump elements) and wideband RCSR performance (75%) are the main advantages of the introduced structure. In the references of Table 1 there is a thin substrate with 0.5 mm thickness. This structure has a very narrowband RCSR performance (about 2% of fractional bandwidth). Therefore, it concludes that there is a trade-off between substrate thickness and RCSR performance. The design of the dual concentrated MS consisting of two MS1 and MS2 (MS1 with RCSR

bandwidth of Δf_1 and MS2 with the RCSR bandwidth of Δf_2) using a gradual phase difference between adjacent cells on a single-layer thin substrate (with 0.8 mm thickness) is one of the main advantages of this structure compared to the state of the art. In simple words, nonconstant PG performance with wideband monostatic RCSR is the main concept of this introduced structure that is certified by measurement result.

Table 1. Comparison between this work and the state-of-the-art.

Structures	Thickness (mm)	BW (%)/ Freq. Rang (GHz)	No of Layers	Substrates
[1]	2.28	85/9.4–23.38	2	RO4003
[2]	5	109/6.4–21.7	3	F4B/Air/F4B
[3]	6.35	60/4.2–7.8	1	RT5880
[5]	2.5	74/7.8–17	1	FR4
[6]	3	82.4/7–16.8	1	RO5880
[7]	0.5	<2/8.9–11.4	1	RO4350
[10]	3	64/9.83–19.12	1	F4B
[11]	3	46/12.1–18.8	1	F4B
This work	0.8	75/20.9–45.7	1	FR4

4. Conclusions

In this paper a new, low-cost, commercially available, simple structure with one layer substrate, thin and wideband dual concentrated MS RCS reducer is introduced. The proposed structure consists of two single bands RCS MS1 and MS2 with RCSR fractional bandwidth of 46% and 40%, respectively. Gradual phase difference between adjacent unit cells on radially modulated surface structure is the main concept behind the MS1 and MS2 design that causes nonconstant PG along the surface that efficiently redirects the incident wave. Placing two PG MS1 and MS2 in the concentrated configuration with one-layer thin substrate (0.8 mm) increases the monostatic RCSR bandwidth up to 75% (20.9–45.7 GHz), which is verified by measurement results.

References

1. Esmaeli, S.; Sedighy, S. Wideband Radar Cross-Section Reduction by AMC. *Electron. Lett.* **2016**, *52*, 70–71. [CrossRef]
2. Xue, J.; Jiang, W.; Gong, S. Wideband RCS Reduction of Slot-Coupled Patch Antenna by AMC Structure. *Electron. Lett.* **2017**, *53*, 1454–1456. [CrossRef]
3. Chen, W.; Balanis, C.A.; Birtcher, C.R. Checkerboard EBG Surfaces for Wideband Radar Cross Section Reduction. *IEEE Trans. Antennas Propag.* **2015**, *63*, 2636–2645. [CrossRef]
4. Shi, H.; Li, J.; Zhang, A.; Jiang, Y.; Wang, J.; Xu, Z.; Xia, S. Gradient Metasurface with Both Polarization-Controlled Directional Surface Wave Coupling and Anomalous Reflection. *IEEE Antennas Wirel. Propag. Lett.* **2015**, *14*, 104–107. [CrossRef]
5. Li, Y.; Zhang, J.; Qu, S.; Wang, J.; Chen, H.; Xu, Z.; Zhang, A. Wideband Radar Cross Section Reduction Using Two-Dimensional Phase Gradient Metasurfaces. *Appl. Phys. Lett.* **2014**, *104*, 221110. [CrossRef]
6. Zhang, W.; Liu, Y.; Gong, S.; Wang, J.; Jiang, Y. Wideband RCS Reduction of a Slot Array Antenna Using Phase Gradient Metasurface. *IEEE Antennas Wirel. Propag. Lett.* **2018**, *17*, 2193–2197. [CrossRef]

7.   Cheng, Y. An Ultra-Thin Dual-Band Phase-Gradient Metasurface Using Hybrid Resonant Structures for Backward RCS Reduction. *Appl. Phys. A* **2017**, *123*, 143. [CrossRef]

8.   Azizi, Y.; Soleimani, M.; Sedighy, S.H. Low Cost, Simple and Broad Band Radar Cross Section Reduction by Modulated and Holography Metasurfaces. *J. Phys. D Appl. Phys.* **2019**, *52*, 435003. [CrossRef]

9.   Liu, Y.; Hao, Y.; Li, K.; Gong, S. Wideband and Polarization-Independent Radar Cross Section Reduction Using Holographic Metasurface. *IEEE Antennas Wirel. Propag. Lett.* **2015**, *15*, 1028–1031. [CrossRef]

10.   Zheng, Q.; Li, Y.; Zhang, J.; Ma, H.; Wang, J.; Pang, Y.; Han, Y.; Sui, S.; Shen, Y.; Chen, H.; et al. Wideband, Wide-Angle Coding Phase Gradient Metasurfaces Based on Pancharatnam-Berry Phase. *Sci. Rep.* **2017**, *7*, srep43543. [CrossRef]

11.   Feng, M.; Li, Y.; Zheng, Q.; Zhang, J.; Han, Y.; Wang, J.; Chen, H.; Sai, S.; Ma, H.; Qu, S.; et al. Two-Dimensional Coding Phase Gradient Metasurface for RCS Reduction. *J. Phys. D Appl. Phys.* **2018**, *51*, 375103. [CrossRef]

12.   Saifullah, Y.; Waqas, A.B.; Yang, G.M.; Zhang, F.; Xu, F. 4-Bit Optimized Coding Metasurface for Wideband RCS Reduction. *IEEE Access* **2019**, *7*, 122378–122386. [CrossRef]

13.   Azizi, Y.; Soleimani, M.; Sedighy, S.H. Ultra-wideband radar cross section reduction using amplitude and phase gradient modulated surface. *J. Appl. Phys.* **2020**, *128*, 205301. [CrossRef]

14.   Yu, N.; Capasso, F. Flat optics with designer metasurfaces. *Nat. Mater.* **2014**, *13*, 139–150. [CrossRef] [PubMed]

15.   Monebhurrun, V. IEEE Standard 1502-2020: IEEE Recommended Practice for Radar Cross-Section Test Procedures [Stand on Standards]. *IEEE Antennas Propag. Mag.* **2021**, *63*, 106. [CrossRef]